NATIONAL RADIO ASTRONOMY OBSERVATORY
Green Bank, West Virginia

ELECTRONICS DIVISION INTERNAL REPORT NO. 309

CALIBRATING THE GBT FOR SPECTRAL POLARIMETRY USING CROSS CORRELATION

Carl Heiles, Rick Fisher

June 21, 1999

CALIBRATING THE GBT FOR SPECTRAL POLARIMETRY

USING CROSS CORRELATION

Carl Heiles, Rick Fisher

ABSTRACT

We outline some aspects of the observational theory and practice of calibrating and observing spectral polarimetry using cross-correlation, with emphasis on measuring the Stokes V required for Zeeman splitting. We consider two cases: **(1)** crosscorrelating a dual-linear feed, and **(2)** using a dual-circular feed with a hybrid and crosscorrelating the resulting linears. We derive the Mueller matrices for these cases; they are completely derivable from astronomical measurements, and we discuss the techniques required. We provide two catalogs of polarization results for sources that can be used as single-dish calibrators, one for 1420 MHz and one for the $4 \rightarrow 15$ GHz region.

With crosscorrelation, both the amplitude and phase of the system must be accurately calibrated with noise injection. As we discuss in sections **3.2** and **4.9**, we require a correlated cal that can be injected in three different ways: into both channels simultaneously, and into each of the two channels independently. For the dual-linear case it is convenient for the relative phase to be approximately the same as that of a linearly polarized astronomical source. For the dual-circular/hybrid case the cal phase should be adjusted to zero output in one of the post-hybrid linear channels.

The injected noise is similar in character to what we are trying to measure; this means that it should not be turned on during an observation. Rather, it should be turned on briefly before and after each observation. It should be strong enough so that a brief integration produces accurate results.

Polarization measurement by cross correlation requires phase stability. All local oscillators must be phase stable with the same requirements as used in interferometry. Traditionally this is not a consideration for spectrometers. We found that an oscillator in the spectral processor was not phase stable.

It is almost impossible to know the polarization response of a cross-correlation polarimeter without a known source. For linear polarization we can use astronomical calibration sources. However, for circular polarization we need a local radiator, such as a helix; because it is used only to establish the sense of polarization, it need not have exquisitely high polarization purity.

1. INTRODUCTION

We write this memo in terms of our interest in Zeeman splitting, which needs the Stokes V (circularly polarized) component. The traditional method for measuring Zeeman splitting with single-dish radio astronomy is switching between the two circular polarizations. This method developed historically because it is conceptually simple and can be used with almost any spectrometer. However it is not the optimum technique. For best performance the switch must be placed in front of the first amplifier, where it adds noise. Also the accuracy of the polarization adjustment is usually not very high.

In radio interferometry, it is well known that the most accurate way to measure circular polarization is to cross correlate two orthogonal linears. This technique can also be used with single-dish spectroscopy if the spectrometer has the capability. While this technique eliminates the noisy switch, it has a basic calibration requirement: at the input to the spectrometer, one must know the *relative phase* of the two linear polarizations. This is equivalent to calibrating the difference in cable length for the two polarizations.

At the GBT, feeds below 8 GHz are intrinsically linearly polarized and the straightforward crosscorrelation described above applies. However, above 8 GHz the feeds are intrinsically circularly polarized and there is no polarization switch before amplification. To generate the Stokes V there are two options: **(1)** polarization switch after amplification, or **(2)** generate linear polarizations with a hybrid and correlate these two linears.

Method **(1)** has the basic technical requirement that the gains of the amplifiers before the switch be identical. Otherwise, a replica of the Stokes I appears in the switched Stokes V spectrum. Method **(2)** has the same requirement plus one more: the phase difference between the amplifiers should be zero. Stennis (1999) has investigated the stability of these amplifiers in the laboratory and found that both the relative gain and phase are stable. Thus either method should work.

Based on our recent observing experiences, we prefer method **(2)**. Firstly and most importantly, it allows one to derive Stokes V by cross correlation instead of differencing the two circular polarizations, which are large numbers. This means that the bandpass correction operates only on the Stokes V itself, which in turn means it need not be known accurately—in spectropolarimetry, Stokes V is weak and the errors are always dominated by noise and other instrumental effects. We note that the bandpass shape comes mainly from the i.f. portions of the system, which come after the hybrid; this means that, indeed, they do not enter the cross-correlation spectra except as a gain error. Secondly, method **(2)** provides all Stokes parameters and one has after-the-fact control over the polarization calibration by frequently using a correlated noise source. Thirdly, spectral lines can be linearly polarized, for example if they are in absorption against a linearly polarized radio source; if one doesn't measure this linear polarization and some linear leaks into the circular, then one observes pseudo-circular and has no idea that it might result from such leakage. Method **(1)** provides none of these advantages.

This memo discusses some basic aspects of the theory and practice of these calibrations. It is based on our experience using the spectral processor in three observing sessions with the 140 foot telescope and on one extensive session at Arecibo in February 1999. Two of the 140-foot sessions were at 1.4 GHz (Apr 1998 and Jan 1999), crosscorrelating two linears, and one at 9.5 GHz using a dual-circular feed and hybrid (May 1999). We learned about small instrumental effects that can affect the astronomical measurements unless they are properly calibrated and equipment details that need to be accounted for in the calibration. We also measured the polarization properties of linearly polarized sources so that they can be used as calibration sources.

We begin in section 2 with a description of the 4 × 4 Mueller matrices and their associated Jones matrices, which relate the output to the input Stokes parameters for the various elements of the system. Section 3 gives the Mueller matrix for a linearly polarized feed and section 4 derives it for a circularly polarized feed with hybrid. Section 5 discusses the practical details of calibrating the relative phase. Section 6 discusses the relevant hardware aspects of the spectral processor. Section 7 discusses our experiences and results relevant to the hardware, with emphasis on the problems. Section 8 presents our catalogs of calibration sources for 1.4, 4, 8, and 14 GHz, together with the observational and data reduction techniques.

2. OUR SCHEME OF MUELLER MATRICES

The key to making accurate polarization measurements is calibration of the four Stokes parameters. Generally, any device has a Stokes-parameter transfer function that relates the output parameters S_{out} to the inputs S_{in}. This is called the Mueller matrix M:

$$\mathbf{S_{out}} = \mathbf{M} \cdot \mathbf{S_{in}} \ . \tag{1}$$

Here **S** is the usual 4-element Stokes parameter vector

$$\mathbf{S} = \begin{bmatrix} I \\ Q \\ U \\ V \end{bmatrix} \ . \tag{2}$$

The Mueller matrix is a 4 × 4 matrix in which all elements may be nonzero. In the usual way, we write

$$\mathbf{M} = \begin{bmatrix} m_{II} & m_{IQ} & m_{IU} & m_{IV} \\ m_{QI} & m_{QQ} & m_{QU} & m_{QV} \\ m_{UI} & m_{UQ} & m_{UU} & m_{UV} \\ m_{VI} & m_{VQ} & m_{VU} & m_{VV} \end{bmatrix} . \tag{3}$$

The matrix elements are just the partial derivatives, for example

$$m_{IQ} = \left| \frac{\delta I}{\delta Q} \right|_{U,V} . \tag{4}$$

The observing system consists of several distinct elements. Each has its own Mueller matrix. Here we consider four, which we consider in sequence as seen by the incoming radiation. We have the feed matrix $\mathbf{M_F}$, the first-amplifier matrix $\mathbf{M_{A1}}$, possibly a hybrid matrix $\mathbf{M_H}$, and the second-amplifier matrix $\mathbf{M_{A2}}$. Sometimes additional matrices are required to convert measured quantities to the standard definitions. The system Mueller matrix is the product of them all in the proper sequence; for our four including the hybrid, $\mathbf{M_{tot}} = \mathbf{M_{A2}} \cdot \mathbf{M_H} \cdot \mathbf{M_{A1}} \cdot \mathbf{M_F}$.

We derive these matrices by considering how the devices affect the amplitude and phase of the voltages in the two polarization channels. We represent the two complex voltages by a vector, and each system component has a voltage transfer function which is a 2 × 2 matrix. These are referred to as Jones vectors and matrices (Tinbergen 1996). Each Jones matrix has its Mueller matrix counterpart. It is straightforward to relate the two types of matrix, once we first define how we measure and calculate the Stokes parameters from the voltages in the two polarization channels. Below we consider the dual-linear and dual-circular cases separately.

While discussing definitions we emphasize Stokes V. We follow the IEEE definition, namely

$$V = LCP - RCP \tag{5}$$

where LCP means left-hand-circular polarization. LCP is generated by transmitting with a left-handed helix, so from the transmitter the E vector appears to rotate anticlockwise. From the receiver, LCP appears to be rotating clockwise.

Astronomical sources don't exhibit much circular polarization so we must define the sense of V by radiating a calibration signal with a helical radiator, being sure to account for a reversal in sense upon each reflection. One sets $m_{VV} = \pm 1$ depending on the results.

3. THE GBT BELOW 8 GHZ: THE MUELLER MATRIX FOR AN INTRINSICALLY LINEAR FEED + AMPLIFIER

3.1. The Mueller matrix

For a good feed the Mueller matrix has important symmetries. "Good" means that we get acceptable accuracy with the first-order expansion of the Jones matrix (e.g. equation 8 below). Heiles (1999) has treated this case in some detail, so here we just provide the results and a quick summary.

We take the Jones matrix identical to that for a dual-circular feed in equation 8 below, with the exception that the subscripts (R, L), which designate the orthogonal circular polarizations, are instead (X, Y), which designate orthogonal linears. We calculate Stokes parameters as follows:

$$I = E_X \bar{E}_X + E_Y \bar{E}_Y \tag{6a}$$

$$Q = E_X \bar{E}_X - E_Y \bar{E}_Y \tag{6b}$$

$$U = E_X \bar{E}_Y + E_Y \bar{E}_X \tag{6c}$$

$$iV = E_X \bar{E}_Y - E_Y \bar{E}_X \tag{6d}$$

where $i = \sqrt{-1}$ and the bar over a symbol indicates the complex conjugate.

With astronomical measurements we cannot separate the feed from the amplifiers. Rather, we can only determine their product. Retaining the first-order terms only, it is

$$\mathbf{M_{A+F}} = \mathbf{M_A} \cdot \mathbf{M_F} = \begin{bmatrix} 1 & \Delta g & \Sigma\epsilon\cos & \Sigma\epsilon\sin \\ \Delta g & 1 & \Delta\epsilon\cos & \Delta\epsilon\sin \\ \Sigma\epsilon\cos & -\Delta\epsilon\cos & 1 & -\Delta\psi \\ \Sigma\epsilon\sin & -\Delta\epsilon\sin & \Delta\psi & 1 \end{bmatrix} . \tag{7}$$

Here Δg and $\Delta\psi$ are the relative gain and phase difference between the amplifier chains in the two polarization channels; the other parameters describe the feed and are defined below after equation 10. Owing to gain uncertainties we cannot accurately determine the elements on the top row observationally. However, we can obtain the remaining elements from observation by using the rotation of parallactic angle as a linearly-polarized source moves across the sky and performing least square fits.

3.2. Calibrating $\mathbf{M_{A+F}}$ with noise injection

If the noise is injected between the feed and amplifier, then the only nonzero elements in $\mathbf{M_{A+F}}$ are the amplifier terms Δg and $\Delta\psi$. If we inject noise T_{cal} into only one channel then it is equivalent to 100% linear polarization in Stokes Q so $(I,Q) = (+1,+1)T_{cal}$ for injection into X and $(I,Q) = (+1,-1)T_{cal}$ into Y. Application of $\mathbf{M_{A+F}}$ shows that subtraction of the two cases for both I_{out} and also Q_{out} provides a direct measurement of Δg. Alternatively, injecting equal uncorrelated noise into both channels simultaneously gives $(I,Q) = (+1,0)T_{cal}$ and the deflection of Q_{out} again provides a direct measurement of Δg, while the deflections (U_{out}, V_{out}) provide $\Delta\psi$.

To summarize, we can calibrate the amplifier terms of $\mathbf{M_{A+F}}$ with a correlated noise source whose output can be disconnected from each channel separately so that we can make the following three measurements: cal into both channels, cal into L only, cal into R only. We regard this as preferable to using uncorrelated noise, because it is difficult to produce equal uncorrelated noise in the two channels.

4. THE GBT ABOVE 8 GHZ: THE MUELLER MATRICES FOR AN INTRINSICALLY CIRCULAR FEED, AND A HYBRID

4.1. A good circular feed

Here we follow Stinebring (1982), who followed the procedure of Conway and Kronberg (1969) in writing the Jones matrix:

$$\begin{bmatrix} E_{L,out} \\ E_{R,out} \end{bmatrix} = \begin{bmatrix} 1 & \epsilon_1 e^{i\phi_1} \\ \epsilon_2 e^{-i\phi_2} & 1 \end{bmatrix} \begin{bmatrix} E_{L,in} \\ E_{R,in} \end{bmatrix} . \tag{8}$$

Here the ϵ's represent undesirable cross coupling between the two polarizations. This equation assumes that the device under consideration is "good", meaning that we need only retain first-order terms in the voltage gain (but we allow the phase to be arbitrary).

For a dual-circular feed, the incoming sky radiation encounters a feed whose nominal outputs are voltages E_L and E_R. If we insert a hybrid, then the hybrid's output is equivalent to a dual linear feed and converts the voltages to their linearly polarized counterparts E_X and E_Y. This interchanges the definitions of Stokes (U,V) in terms of the voltages (as in equation 6, for example). To avoid confusion, we temporarily forsake using (I,Q,U,V) and instead use (S_0,S_1,S_2,S_3), which we define as follows:

$$S_0 = E_A\bar{E}_A + E_B\bar{E}_B \tag{9a}$$

$$S_1 = E_A\bar{E}_B + E_B\bar{E}_A \tag{9b}$$

$$iS_2 = E_A\bar{E}_B - E_B\bar{E}_A \tag{9c}$$

$$S_3 = E_A\bar{E}_A - E_B\bar{E}_B\,. \tag{9d}$$

As before, $\mathbf{S_{out}} = \mathbf{M}\cdot\mathbf{S_{in}}$. If the system components were perfect, then with the circularly polarized feed before the hybrid $(I,Q,U,V) = (S_0,S_1,S_2,S_3)$ and after the hybrid the order is different, $(I,Q,V,U) = (S_0,S_1,S_2,S_3)$.

With these equations, it is only a matter of a little algebra to calculate the feed's Mueller matrix (this could also be found by a suitable reduction and rearrangement of Stinebring's equation (A.5)):

$$\mathbf{M_F} = \begin{bmatrix} 1 & \Sigma\epsilon\cos & \Sigma\epsilon\sin & 0 \\ \Sigma\epsilon\cos & 1 & 0 & -\Delta\epsilon\cos \\ \Sigma\epsilon\sin & 0 & 1 & -\Delta\epsilon\sin \\ 0 & \Delta\epsilon\cos & \Delta\epsilon\sin & 1 \end{bmatrix}. \tag{10}$$

where $\Sigma\epsilon\cos = \epsilon_1\cos\phi_1 + \epsilon_2\cos\phi_2$; $\Sigma\epsilon\sin = \epsilon_1\sin\phi_1 + \epsilon_2\sin\phi_2$; $\Delta\epsilon\cos = \epsilon_1\cos\phi_1 - \epsilon_2\cos\phi_2$; $\Delta\epsilon\sin = \epsilon_1\sin\phi_1 - \epsilon_2\sin\phi_2$. The good feed is described by only four independent parameters.

One curious comment: the central 4-element submatrix is a rotation matrix that represents an error in position angle of linear polarization. To first order, the nondiagonal elements are zero, which means that the absolute position angle has no uncertainty. This is in contrast to the dual-linear feed, where voltage coupling between the probes makes the nondiagonal elements nonzero. However, any such advantage for measuring linear polarization is illusory, for two reasons: First, with respect to what direction is the position angle measured? Second, amplifiers are necessary, and they introduce phase uncertainty as discussed below.

4.2. The first set of amplifiers

The two polarization channels may or may not go through a hybrid, which converts dual circular to dual linear. However, before the hybrid each goes through the first amplifier chain with gains $G_{L1,R1} = (1 + g_{L1,R1})$ and phase delays $-\psi_{L1,R1}$; here the subscripts L and R denote the circular polarizations and the "1" denotes the first set of amplifiers. To characterize these we rely on careful calibration to make g and ψ small. Retaining only the first-order terms, the associated Jones matrix is

$$\begin{bmatrix} E_{L,out} \\ E_{R,out} \end{bmatrix} = \begin{bmatrix} 1 + g_{L1} + i\psi_{L1} & 0 \\ 0 & 1 + g_{R1} + i\psi_{R1} \end{bmatrix} \begin{bmatrix} E_{L,in} \\ E_{R,in} \end{bmatrix}. \tag{11}$$

and the associated Mueller matrix is

$$\mathbf{M_{A1}} = \begin{bmatrix} 1 & 0 & 0 & \Delta g_1 \\ 0 & 1 & -\Delta\psi_1 & 0 \\ 0 & \Delta\psi_1 & 1 & 0 \\ \Delta g_1 & 0 & 0 & 1 \end{bmatrix} . \tag{12}$$

where $\Delta g_1 = g_{L1} - g_{R1}$ and $\Delta\psi_1 = \psi_{L1} - \psi_{R1}$; also, we have eliminated a factor $(1 + g_{L1} + g_{R1})$ from the diagonal terms because it can be taken care of by intensity calibration and when applied to the off-diagonal terms it is second order.

4.3. The first-amplifier-feed combination

We may or may not use the hybrid. In either case, the incoming signal will first go through the combination of the feed and the first amplifiers. We cannot separate the feed from the first amplifiers, so we calculate the combination. In keeping with our previous approximation of retaining only first-order terms, we obtain

$$\mathbf{M_{A1+F}} = \mathbf{M_{A1}} \cdot \mathbf{M_F} = \begin{bmatrix} 1 & \Sigma\epsilon\cos & \Sigma\epsilon\sin & \Delta g_1 \\ \Sigma\epsilon\cos & 1 & -\Delta\psi_1 & -\Delta\epsilon\cos \\ \Sigma\epsilon\sin & \Delta\psi_1 & 1 & -\Delta\epsilon\sin \\ \Delta g_1 & \Delta\epsilon\cos & \Delta\epsilon\sin & 1 \end{bmatrix} . \tag{13}$$

This matrix has only six independent parameters. It is convenient and helpful that, in this approximation, the matrix elements are caused either by the feed or the amplifiers, but not both.

4.4. The hybrid

The hybrid adds the two incoming voltages, each with a $\frac{\pi}{2}$ phase shift. We assume, also, that the hybrid is imperfect and has small residual losses λ and phase shifts χ in each output. Including these imperfections to first order only makes its Jones matrix

$$\begin{bmatrix} \sqrt{2}E_{A,out} \\ \sqrt{2}E_{B,out} \end{bmatrix} = \begin{bmatrix} 1 & -i(1+\lambda_1)+\chi_1 \\ -i(1+\lambda_2)-\chi_2 & 1 \end{bmatrix} \begin{bmatrix} E_{A,in} \\ E_{B,in} \end{bmatrix} . \tag{14}$$

and the associated Mueller matrix is

$$\mathbf{M_{hybrid}} = \begin{bmatrix} 1 & \Delta\chi & -\Delta\lambda & -\Delta\lambda \\ \Delta\chi & 1 & \Sigma\chi & -\Sigma\chi \\ -\Delta\lambda & \Sigma\chi & -\Sigma\lambda & 1 \\ \Delta\lambda & \Sigma\chi & -1 & -\Sigma\lambda \end{bmatrix} . \tag{15}$$

where $\Sigma\lambda = \frac{\lambda_1+\lambda_2}{2}$, $\Delta\lambda = \frac{\lambda_1-\lambda_2}{2}$, $\Sigma\chi = \frac{\chi_1+\chi_2}{2}$, $\Delta\chi = \frac{\chi_1-\chi_2}{2}$. Again, we have eliminated a factor $(1 + \frac{\lambda_1+\lambda_2}{2})$ from the unitary elements because it can be taken care of by intensity calibration and when applied to the other elements it is second order.

The last two unitary elements do not lie on the diagonal because the hybrid's function is to exchange dual-circular for dual-linear polarization. Note that -1 instead of $+1$ appears in the last row; we will deal with this later.

4.5. The second set of amplifiers

After the hybrid the two polarization channels again go through amplifier chains, and these have transfer matrices that are identical to those of the first set of amplifiers. Thus the associated Mueller matrix for the second set is

$$\mathbf{M_{A2}} = \begin{bmatrix} 1 & 0 & 0 & \Delta g_2 \\ 0 & 1 & -\Delta\psi_2 & 0 \\ 0 & \Delta\psi_2 & 1 & 0 \\ \Delta g_2 & 0 & 0 & 1 \end{bmatrix} . \tag{16}$$

4.6. The Mueller matrix for the whole system with hybrid

The Mueller matrix for the combination of feed, first amplifier, hybrid, and second amplifier is the product of the individual matrices:

$$\mathbf{M_{tot}} = \mathbf{M_{A2}} \cdot \mathbf{M_{hybrid}} \cdot \mathbf{M_{A1+F}} . \tag{17}$$

Even though the hybrid matrix is complicated, retaining first-order terms only makes things fairly simple:

$$\mathbf{M_{tot}} = \begin{bmatrix} 1 & FH & -\mathbf{G_2} & \mathbf{G_1} \\ FH & 1 & \Psi_1 & -\Psi_2 \\ \mathbf{G_1} & \Psi_2 & HF & 1 \\ \mathbf{G_2} & \Psi_1 & -1 & HF \end{bmatrix}, \tag{18}$$

where

$$\mathbf{G_1} = \Delta g_1 - \Delta\lambda \text{ (gain diff of amp 1)} \tag{19a}$$

$$\mathbf{G_2} = \Delta g_2 + \Delta\lambda - \Sigma\epsilon \sin \text{ (gain diff of amp 2)} \tag{19b}$$

$$\Psi_1 = \Delta\psi_1 + \Sigma\chi \text{ (phase diff of amp 1)} \tag{19c}$$

$$\Psi_2 = \Delta\psi_2 + \Sigma\chi + \Delta\epsilon \cos \text{ (phase diff of amp 2)} \tag{19d}$$

$$FH = \Sigma\epsilon \cos + \Delta\chi \text{ (feed gain + hybrid phase)} \tag{19e}$$

$$HF = -\Sigma\lambda + \Delta\epsilon \sin \text{ (hybrid gain + feed phase)} \tag{19f}$$

We have endeavored to make the notation meaningful, using **G** and Ψ for terms containing amplifier gain and phase differences, F and H for feed and hybrid coupling and phase. We have made the amplifier terms prominent with boldface and large Greek letters; they will probably dominate because they are active components and can change with time.

We emphasize that this matrix applies to the Stokes parameter set **S** in equation 9 and because of the hybrid they are not in their usual order. To be explicit, for equation 18 the ordering is

$$\mathbf{S_{out}} = \begin{bmatrix} I_{out} \\ Q_{out} \\ V_{out} \\ U_{out} \end{bmatrix} = \mathbf{M_{tot}} \begin{bmatrix} I_{in} \\ Q_{in} \\ U_{in} \\ V_{in} \end{bmatrix}. \tag{20}$$

Note that $\mathbf{M_{tot}}$ is characterized by six independent elements, the same number that characterizes a feed/amplifier combination without a hybrid. Even though this is a more complicated system, this fact is not so remarkable because the total system is characterized by its own Jones matrix and, after all, the total system is equivalent to a linear feed plus amplifier.

4.7. Summary: a conventional writing of the total system Mueller matrix

As astronomers, we prefer to ignore the details of which component is responsible for which matrix element in equation 18 and, moreover, to write it in the more conventional form in which the Stokes parameters are in the usual order (equation 2). This requires interchanging S_2 and S_3 above, so we designate the resulting total system matrix as $\mathbf{M_{TOT}}$ with the subscript in capital letters. Specifically, then, we define

$$\begin{bmatrix} I_{out} \\ Q_{out} \\ U_{out} \\ V_{out} \end{bmatrix} = \mathbf{M_{TOT}} \begin{bmatrix} I_{in} \\ Q_{in} \\ U_{in} \\ V_{in} \end{bmatrix} . \tag{21}$$

where the primes indicate the measured values and the unprimed parameters the astronomical ones. This is also where we fix the -1 in equation 18:

$$\mathbf{M_{TOT}} = \begin{bmatrix} 1 & 0 & 0 & 0 \\ 0 & 1 & 0 & 0 \\ 0 & 0 & 0 & -1 \\ 0 & 0 & 1 & 0 \end{bmatrix} \mathbf{M_{tot}} . \tag{22}$$

Carrying out the multiplication, we obtain

$$\mathbf{M_{TOT}} = \begin{bmatrix} 1 & FH & -\mathbf{G_2} & \mathbf{G_1} \\ FH & 1 & \Psi_1 & -\Psi_2 \\ -\mathbf{G_2} & -\Psi_1 & 1 & -HF \\ \mathbf{G_1} & \Psi_2 & HF & 1 \end{bmatrix} , \tag{23}$$

This matrix $\mathbf{M_{TOT}}$ has exactly the same form as the Mueller matrix in equation 7, which is for a dual-linear feed plus amplifiers. This identity of form is not surprising because we can consider the combination of the dual-circular feed, first amplifiers, and hybrid as a dual-linear feed; we add the second amplifiers and the system is conceptually identical. This similarity is fortunate, because just as without the hybrid, all of the elements of the total system matrix can be determined observationally and there is no advantage in trying to determine the elements of each system component separately. There is one difference between this case and the dual-linear feed. Here, Stokes Q is derived from the voltage products and U from the power differences; the opposite is true for the dual-linear feed.

4.8. Interpretive discussion of $\mathbf{M_{TOT}}$: practical effects of nonzero matrix elements

In real life the largest terms in M_{TOT} will normally be the ones associated with the amplifiers, G and Ψ.

Zeeman splitting produces weak circular polarization, a weak Stokes V. Matrix elements in the last row are relevant here, and the first two are large because they are associated with the amplifiers. Of these, the term $\mathbf{G_1}$ is most serious because it represents coupling between Stokes I and V, and of course $I \gg V$. The term Ψ_2 represents coupling between linear polarization and V; even if Ψ_2 is large, it won't affect V much because spectral lines exhibit little if any linear polarization.

During our May99 run, we found $G_1 \sim 0.08$. This is large, and would be fatal except for the fact that Zeeman splitting produces a Stokes V that looks like the frequency derivative of the line seen in Stokes I—the famous "S-curve". It is easy, reliable, and accurate to separate the derivative from the line itself in a least squares fit, because the two are nearly orthogonal. The major deleterious effect of nonzero G_1 is an increase in noise, which arises because the noisy bandpass shape appears in the replica of Stokes I that appears in V; the bandpass shape gets removed with the least squares fit, but the noise remains.

If one wanted to measure linear polarization of a spectral line, then there are several important terms arising from the amplifiers. These terms are greatly simplified by eliminating the hybrid.

4.9. Calibrating $\mathbf{M_{TOT}}$ with noise injection

If the noise is injected between the feed and amplifier, then only nonzero elements in $\mathbf{M_{TOT}}$ are the amplifier terms $(\mathbf{G_1}, \mathbf{G_2})$ and (Ψ_1, Ψ_2). We can calibrate these terms by suitable injection of correlated and uncorrelated noise. We consider several cases:

(1) If we inject equal amounts of uncorrelated noise into both channels, then all Stokes parameters except I are zero. Application of $\mathbf{M_{TOT}}$ shows that the deflections of (U_{out}, V_{out}) provide direct measurements of $(\mathbf{G_2}, \mathbf{G_1})$.

(2) If we inject noise T_{cal} into only one channel then it is equivalent to 100% circular polarization in Stokes V so $(I, V) = (+1, +1)T_{cal}$ for injection into channel L and $(I, Q) = (+1, -1)T_{cal}$ for channel R. Application of $\mathbf{M_{TOT}}$ shows that for either case U_{out} provides $\mathbf{G_2}$ and Q_{out} provides Ψ_2 (doing both cases is not necessary). Also, the deflections of (I_{out}, V_{out}) are identical and subtraction of the two cases provides $\mathbf{G_1}$. In summary, doing both cases provides measurements of $(\mathbf{G_1}, \mathbf{G_2}, \Psi_2)$ but not Ψ_1.

(3) If we inject equal amounts of correlated noise into both channels, then this is equivalent to linear polarization with a position angle that depends on the relative phase. In our May99 run, this cal phase was adjusted to give $Q = 0$ and $(I, U) = (+1, +1)T_{cal}$. Application of $\mathbf{M_{TOT}}$ shows

that the deflection Q_{out} provides Ψ_1 and V_{out} provides $\mathbf{G_1}$. Note that this scheme with Q_{out} is the only way to obtain Ψ_1. However, in the final analysis Ψ_1 determines position angle on the sky and its absolute value must be determined astronomically.

In summary, we can use cases **(1)** and **(2)** to calibrate the amplifier terms of $\mathbf{M_{TOT}}$, i.e. use a correlated noise source whose output can be disconnected from each channel separately so that we can make the following three measurements: cal into both channels, cal into L only, cal into R only. We regard this as preferable to case **(1)** because it is difficult to produce equal uncorrelated noise in the two channels.

4.10. Calibrating the noise source and the complete Mueller matrix using astronomical sources

The above section describes the calibration procedure injecting noise just after the feed. However, the noise source is not a primary calibration standard. Furthermore, it cannot calibrate the properties of the feed. These aspects require calibration using astronomical observations. These are fully discussed by Heiles (1999); below we give a brief summary.

5. PRACTICAL CONSIDERATIONS

5.1. Observational determination of the Mueller Matrices

The elements on the top row of the Mueller matrix are not easily measurable because they reflect the imperfections in the system that convert polarized intensity, which is small, to total intensity, which is large. Moreover, as we track a source the zenith angle changes. The effective telescope gain depends on zenith angle, at least because of atmospheric attenuation and possibly because of variations in telescope gain because of time, temperature, or gravitational distortion; even if they are small, these effects are likely to be at least comparable to the imperfections of cross-polarization coupling. The resulting covariance between parallactic angle and telescope gain makes the top-row elements underivable directly from observations.

This gain uncertainty has one additional ramification. It affects not only Stokes I but the other Stokes parameters as well—they all scale directly with the telescope gain. These gain variations would affect the least square fits. This effect is probably not important in practice, but we can easily avoid this problem by using the Stokes parameters expressed in units of I, i.e. using fractional polarization.

To measure the elements of the Mueller matrices one follows the prescription of Heiles (1999) in detail; here we provide the briefest of summaries. One selects a sample of linearly polarized calibration sources and does ON-OFF measurements from horizon to horizon, which maximizes

the position angle coverage by parallactic angle. One assumes the sources have zero circular polarization. By performing least square fits, one determines the measured polarization of each source.

For the intrinsically linear feed, the system's linear polarization directions are determined by the mechanical mounting of the feed and a cross-coupling term. These should be small, so unless one is interested in highly accurate absolute position angles one can neglect these corrections and avoid relying on previously-determined source position angles; with this, the calibration is completely internal. However, for the intrinsically circular feed the system's directions depend on the relative phase difference between the two circulars. Therefore, proper calibration requires knowledge of the calibration source position angles of linear polarization. Apart from this difference, the details of the fitting are similar to those for the intrinsically linear case, and we won't take the space to describe them here but instead refer to Heiles (1999).

One must take care to include all Mueller matrices that describe the various components of the complete system. For example, at Arecibo the definition of Stokes parameters in the on-line datataking software differed from the conventional one and we had to define an additional matrix in which one of the elements is -1. It is important to obtain final Stokes parameters that are defined conventionally, and it is best to incorporate all corrections into the final matrix so that no additional *ad-hoc* corrections are required.

5.2. Deriving the relative phase using astronomical sources

In this section we describe how to derive the relative phase of a correlated signal. We assume linear polarizations, but the discussion applies equally for circulars.

We denote the signals from the two orthogonally linearly polarized feeds by **X** and **Y**. The spectral processor provides the Fourier transform-derived cross product power spectrum. This consists of the real and imaginary portions of the cross power spectrum, which are precisely 90 degrees out of phase; we denote these by Re(**XY**) and Im(**XY**). We need Re(**XY**) to correspond to Stokes U and Im(**XY**) to Stokes V. In this case, linear polarization would produce output only in Re(**XY**) and circular in Im(**XY**). This is exactly the condition we need to attain by calibration. To perform this calibration, we use a source of correlated noise in the two channels—a correlated noise source, or CCAL.

If we observed an unpolarized continuum radio source, then $\mathbf{XY} = 0$. Some continuum sources have significant linear polarization; in this case, **XY** is nonzero. If we observe a selection of linearly polarized sources and plot the results in the [Re(**XY**), Im(**XY**)] plane, we obtain something like Figure 1, which are actual observations for three sources each observed at 12 position angles over a range of 360°, during our Jan99 run. These data exhibit a well-defined slope and go through zero (almost). Note in particular that the slope is independent of the position angle of the source polarization and also of the feed. The slope depends only on the relative phase

between **X** and **Y** as they enter the spectral processor, and because the correlated signal from the linearly-polarized source hits the two feeds at the same time no matter what the position angles are, the phase difference between **X** and **Y** is constant.

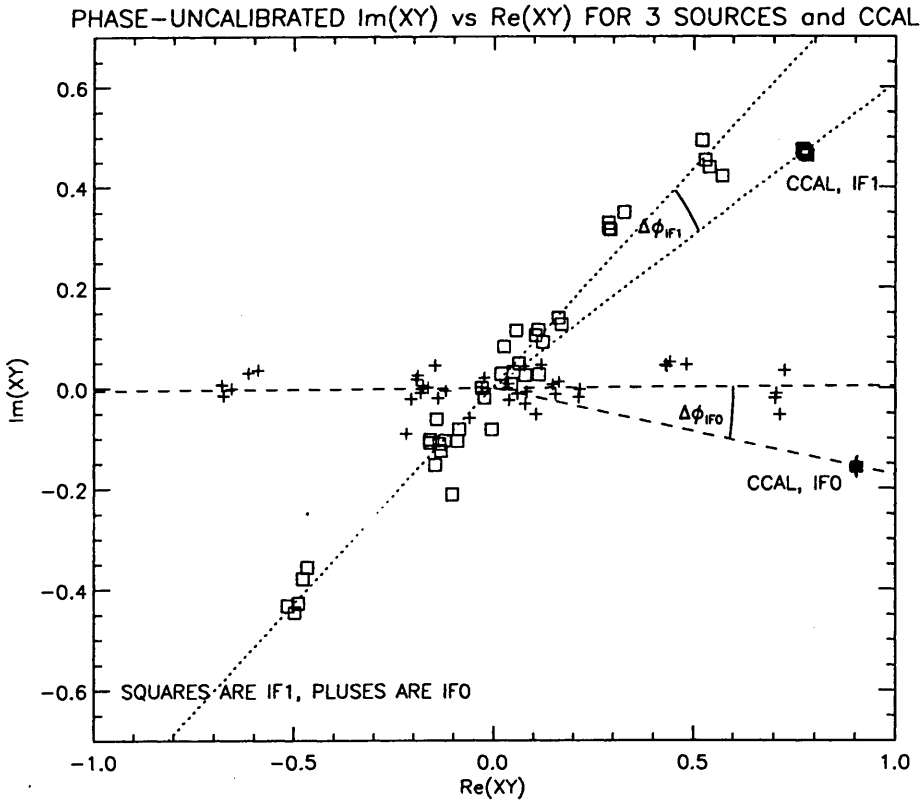

Fig. 1.— Im(**XY**) versus Re(**XY**) for three linearly polarized sources (3C227, 3C270, 3C273) and also for the CCAL. Each source was observed at 12 different feed position angles that covered a range of 360°. Squares and dotted lines are for IF1, pluses and dashed lines are for IF0. The phase differences $\Delta\phi$ for IF0 and IF1 are −10.0° and −9.5°, which are equal to within the uncertainties, and the angles ϕ_{SRC} are 0.3° and 40.8°; the small value of ϕ_{SRC} for IF0 is pure happenstance.

In Mueller matrix terms, the slope is $\tan^{-1} m_{VU}$ and the zero offset caused by m_{VI}, m_{VQ}, m_{UI}. The slope does not depend on the details of source polarization or feed position angle, as long as the polarization is linear. Rather, the slope depends on the relative phase delay between the feeds and the spectral processor, which depends on the difference in cable length. It is this relative phase delay that we need to calibrate. The data in Figure 1 are sufficient to calibrate this relative delay. These astronomical data are *primary calibration data* because they are absolute measurements of astronomical sources and sufficient, in themselves, for this calibration.

Although these sources provide primary calibration data, using them for system calibration on a routine basis is inconvenient. From the practical standpoint, we always prefer to calibrate with a noise source that can be turned on and off because it is quick and convenient. To calibrate the phase difference, it is clear that we need a source of correlated noise at the feed. This is a *secondary calibrator* because it must be calibrated by comparison with astronomical sources.

5.3. Deriving the relative phase using the correlated cal

If we inject correlated noise into the two channels with the CCAL, then there is perfect correlation and **XY** is large. If the relative phase of this correlated noise, as injected into the system, were the same as the relative phase of correlated noise from linearly polarized astronomical sources, then it would produce points that lie on the slope defined by those sources. However, such a zero-difference condition is difficult to achieve. Thus the CCAL points define a different slope.

In Figure 1, we show independent results for identical observations with the two IF channels IF1 and IF0. For each IF, the CCAL points form an angle ϕ_{CCAL} and the source points ϕ_{SRC}. The difference between these two angles $\Delta\phi = \phi_{SRC} - \phi_{CCAL}$ is the same for the two IF's because it depends only on the details of how the CCAL is injected, for example the exact cable lengths connecting the CCAL to the two system inputs. If these details are unchanged, then $\Delta\phi$ should remain constant (and indeed we found it to be constant, both at Green Bank and Arecibo). Suppose we determine this angle accurately by an extensive series of observations of linearly polarized sources. Then we can calibrate the system with the CCAL, because when we determine ϕ_{CCAL} it is the same as determining ϕ_{SRC}.

5.4. A practical point: least square fitting the points in Figure 1

It is conceptually easy to fit the source points in Figure 1 with a straight line and determine their slope, and then do the same for the CCAL points; this provides the necessary quantity $\Delta\phi$. However, the details of the least square fitting process do not favor this particular method. One reason is that the least-square fitting process regards the points on the horizontal axis as the independent variable, measured with high accuracy, and those on the vertical axis as the dependent variable, measured with low accuracy; it does not treat the two sets of data impartially. Moreover, suppose for example that $\phi_{SRC} \sim 90°$; then the least square process, which assumes that the points on the horizontal axis are the well-known independent variable, breaks down completely.

A simple alternative that works well is to transform the variables and plot the difference $D = [\mathrm{Re}(\mathbf{XY}) - \mathrm{Im}(\mathbf{XY})]$ versus the sum $S = [\mathrm{Re}(\mathbf{XY}) + \mathrm{Im}(\mathbf{XY})]$. In this space, the angle of the points from the horizontal axis never exceeds 45° and, moreover, neither $\mathrm{Re}(\mathbf{XY})$ nor $\mathrm{Im}(\mathbf{XY})$ is favored. If the slope of the least-square fitted line of D versus S is B, then it is clear that the

corresponding angle in Figure 1 is given by

$$\tan\phi = \frac{1-B}{1+B}\,. \tag{24}$$

5.5. Phase variation across the observing band

The system phase varies across the observing band. Figure 2 shows the CCAL deflection over a 10 MHz bandwidth for two scans near the beginning and end of the Jam99 observing run. The phase variation in the two scans is nearly identical apart from a constant offset. The phase changes slowly with channel number by a total of about 40°. This change is mainly linear with frequency. Such a linear phase change is produced by different cable lengths in the two polarization channels. For spectral line observations it is crucial to account for this in the bandpass calibration. For continuum observations at wide bandwidth, the cable lengths must be made sufficiently identical to avoid cancellation of the correlated signals within the band.

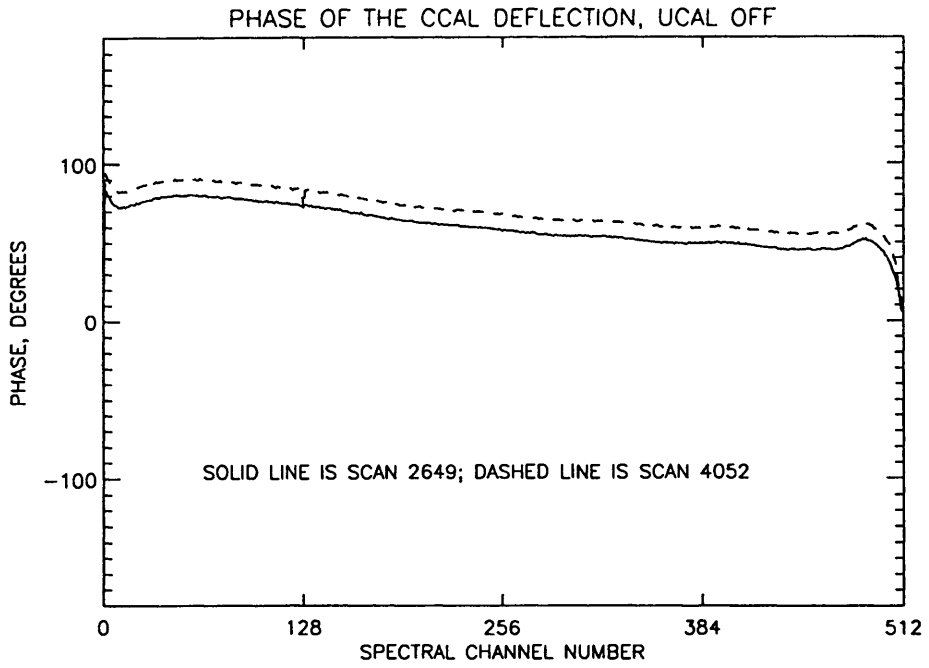

Fig. 2.— Frequency dependence of CCAL phase ϕ_{CCAL} in IF1 for 10 MHz bandwidth versus spectral channel number for two scans near the beginning and end of the week's observing run. The small spike in channel 128 comes from a polarized calibration signal radiated from a vertex antenna.

There also seems to be a nonlinear aspect to the phase variation with frequency. This appears to mimic the bandpass shape in that it changes most rapidly at the edges, so it probably occurs within the spectral processor, presumably because of small differences between the filters in the two channels.

5.6. Another practical point: a robust least square fit of the phase versus frequency

Mostly, the phase varies linearly with frequency, and one wants to determine and remove this slope. Here we are discussing ϕ_{SRC} and ϕ_{CCAL}, not their difference $\Delta\phi$, which should be almost independent of frequency. To determine this slope, the knee-jerk response is to linearly fit ϕ_{CCAL} to frequency. However, this isn't straightforward because ϕ_{CCAL} suffers sudden wraparound jumps of 2π when it crosses the boundaries $-\pi$ or π. We offer the following robust prescription.

First, from Figure 1 realize that

$$\phi_{CCAL} = \tan^{-1}\left[\frac{\mathrm{Im}(\mathbf{XY})}{\mathrm{Re}(\mathbf{XY})}\right] , \tag{25}$$

which means that $\sin\phi_{CCAL} = \mathrm{Im}(\mathbf{XY})$ and $\cos\phi_{CCAL} = \mathrm{Re}(\mathbf{XY})$. We write

$$\phi_{CCAL} = A + Bf \tag{26}$$

where f is the r.f. frequency and (A, B) are the constants we need to determine. Write

$$\cos(A + Bf) = C\cos(Bf) + D\sin(Bf) \tag{27a}$$

$$\sin(A + Bf) = C'\cos(Bf) + D'\sin(Bf) \tag{27b}$$

and determine (B, C, D, C', D'). Including B in a standard least-squares is distasteful for two reasons: firstly, it's a nonlinear least-squares fit; secondly, B is likely to be indeterminate because Bf probably won't change much across the observing band.

To deal with this in a robust way perform the following steps in sequence:

(1) Estimate an approximate value for B. This parameter depends on cable length differences and should remain constant with time. For a well-constructed system it is small. If ϕ_{CCAL} doesn't change much over the observing band, such as in Figure 2, it's OK to use $B = 0$.

(2) Using this estimated value for B, fit for (C, D, C', D') in equation 27. Note that these are linear least squares fits.

(3) Use the fit to equation 27 to define the residuals

$$R = \phi_{CCAL} - \tan^{-1}\left[\frac{C'\cos(Bf) + D'\sin(Bf)}{C\cos(Bf) + D\sin(Bf)}\right] \tag{28}$$

R contains a residual slope that reflects the error in your estimate of B. These residuals are centered on $R = 0$ and should all lie well within the range $-\pi \rightarrow \pi$. Because there are no sudden jumps from wraparound, the slope can be obtained from a linear least squares fit.

6. THE SPECTRAL PROCESSOR

6.1. DESCRIPTION

The Green Bank spectral processor is a Fourier-transform spectrometer whose digital hardware computes real-time FFT's on the baseband voltage samples of any receiver's IF signal. The spectral processor contains two FFT engines with a common clock and timing circuitry. Each FFT engine can accept 1, 2, or 4 sampled IF inputs to produce spectra with 1024, 512, or 256 frequency points, respectively, from each IF. The complex voltage spectra from the two FFT engines may be cross multiplied as shown in Figure 3.

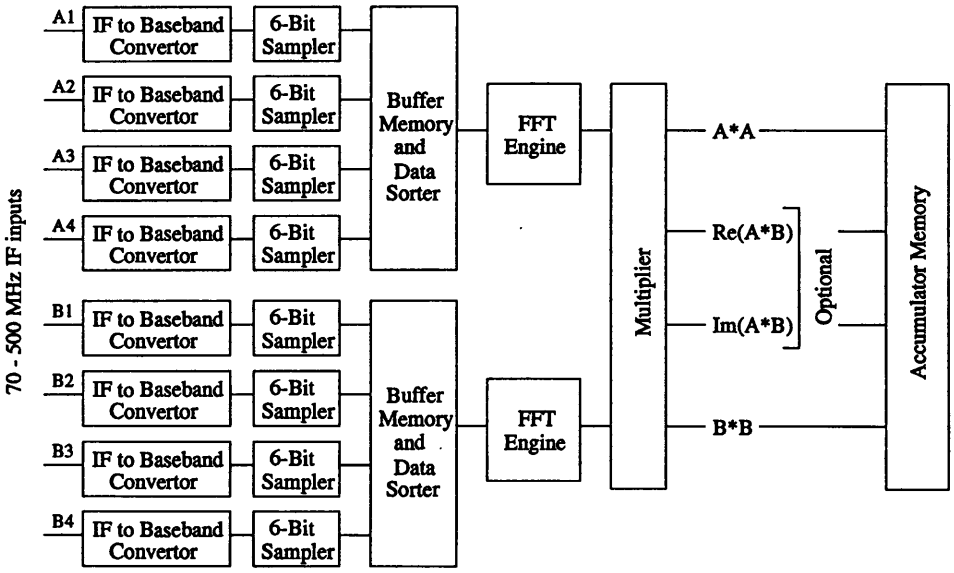

Fig. 3.— Spectral Processor block diagram

When only the self-products are computed (A*A and B*B in Figure 3) the total FFT bandwidth of each engine is 40 MHz (80 real mega-samples per second) which may be divided between the 1, 2, or 4 IF inputs. In other words, if 4 IF samples are being accepted by one FFT engine, the maximum bandwidth of each IF spectrum is 10 MHz. If both self- and cross-products are computed, the total bandwidth must be 20 MHz or less.

Our polarization measurement tests used 2 IF's on each FFT engine (A1, A2, B1, and B2), each with a bandwidth of 10 MHz, and all products were computed and stored. The signal from one linear polarization was split and sent to inputs A1 and A2, and the other polarization was sent to B1 and B2. Both spectrum pairs, A1/B1 and A2/B2 were centered at the same frequency as a redundancy check on the independent IF components and samplers.

Let g be the ratio of the gain of channel A to the gain of channel B as a function of frequency across the spectrum. Then, if A and B are connected to orthogonal, linearly polarized feed outputs, the Stokes parameters may be computed from the spectral processor output spectra as follows:

$$I = A * A + gB * B \tag{29}$$

$$Q = A * A - gB * B \tag{30}$$

$$U = 2\sqrt{g}Re|A * B| \tag{31}$$

$$V = -2\sqrt{g}Im|A * B| \tag{32}$$

There are a number of calibrations and corrections that must be applied to the data before these equations are valid. Those corrections are the subject of other sections of this report.

At the two FFT outputs, the relative phase of the signal that is correlated between channels A and B is given by

$$Phase = \arctan \frac{Im|A * B|}{Re|A * B|} \tag{33}$$

This phase depends on the cable lengths, relative phases of the synchronous or common LO's, and the filter phase shifts in the two IF channels. This instrumental phase must be measured with a common noise signal injected into the input to the two receiver channels.

A mystery that has been with the spectral processor since its inception is that, for a correlated input signal, the amplitude of the correlated output is almost always less that the sum of the self-products of the same signal in channels A and B. A typical loss is a few percent, but it can be as high as 10%. This loss is corrected in the calibration procedures, but its existence is bothersome. At various times during the life of the spectral processor attempts have been made to associate the loss of correlation with input signal level, combinations of IF modules, input signal phase, and other variables, but the puzzle remains.

6.2. INTERNAL L.O. AND ELECTRONICS PHASE STABILITY

There are two local oscillators in each IF convertor section of the spectral processor. The first is a tunable LO (230 to 660 MHz) that converts an input signal with a frequency anywhere between 70 and 500 MHz to an intermediate IF that is either the upper or lower sideband of 160 MHz. The second LO is fixed at 160 MHz and converts the signal to baseband with a single-sideband mixer. Both of these LO's use a 5 MHz signal from the site maser as a phase reference.

Any phase noise in either of these LO signals will cause a loss of coherence between two IF channels so we suspected this as the source of coherence loss mentioned above. To test this we injected a common CW signal into the input of two IF sections at a frequency that converted to 100 kHz at baseband. The two 100 kHz signals were then compared with an oscilloscope. The largest peak-to-peak phase noise between any two IF sections was 40 degrees or about 8 degrees rms. This would explain only about 1% loss of coherence so it does not appear to be the major cause of correlation loss. When a common LO signal was substituted for the internal variable oscillators the phase noise dropped to less than 5 degrees peak-to-peak. This indicates that most of the phase noise is coming from the internal variable LO's.

During our first observations in April 1998 we saw a number of substantial phase calibration jumps of as much as 40 degrees from one day to the next. To determine whether these phase changes were happening in the spectral processor electronics we measured the relative phase of a common noise signal through channels A1 and B1 and channels A2 and B2 over about two hours while the temperature of all or part of the electronics was varied by opening and closing rack drawers and covering individual IF drawer vents. No relative phase changes greater than 1.6 degrees were measured.

On the first day of the January 1999 observations a substantial phase jump was seen in the calibration of the A1/B1 IF pair as measured with the correlated noise cal. The phase of IF pair A2/B2, which was connected to the same IF signals at the same frequency, was stable during this period. For second and following days of this run and for the May 1999 run we used a common external oscillator for the variable LO of IF channels A1 and B1. No further phase jumps were seen.

6.3. TRANSFER CHARACTERISTICS

To check the linearity of the samplers (six-bit A/D's) in the spectral processor we took a series of spectrum measurements at different input power levels to the samplers while the telescope was looking at cold sky. The input power level was varied by changing the IF attenuators in the IF to Baseband Convertor modules. These attenuators have nominally 1 dB steps and are accurate to about 0.1 dB. The input power levels were varied from about 6 dB below the normal operating level to about 6 dB above. The measured power transfer functions for the four IF channels are shown in Figure 4.

The horizontal axis in Figure 4 is the log of the relative input power to each sampler as determined by the attenuator setting. The points for the four IF channels are arbitrarily offset in the horizontal direction for so that they are not confused in the plot. The vertical axis is the log of the output power of the FFT as measure by the median power of the 512 channels in each spectrum. The straight line associated with each set of measurements has a slope of one and is adjusted to have a zero average vertical deviation from the plotted points. To the extent that

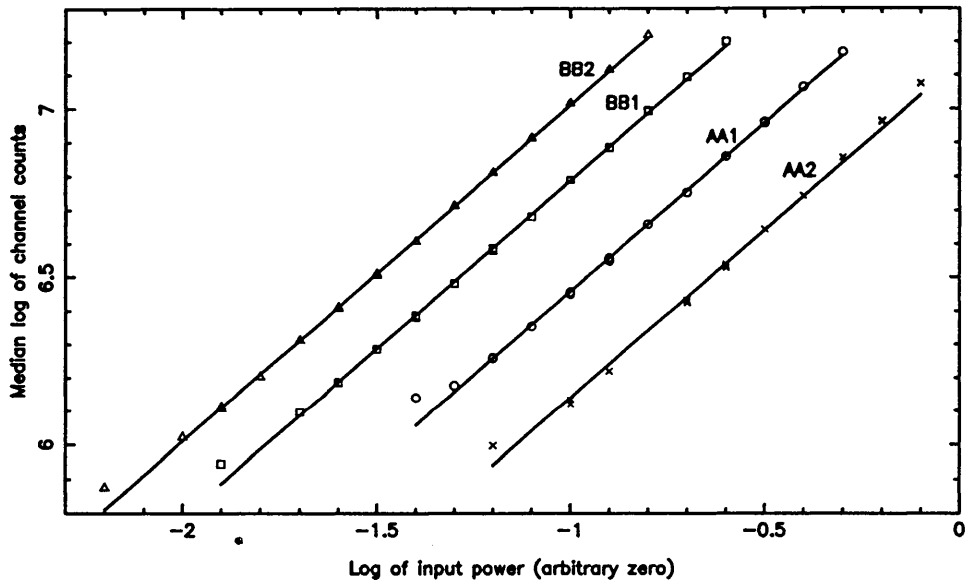

Fig. 4.— Spectrum output power as a function of input noise power. The normal operating point for the A/D's is at $log(outputpower) \approx 6.55$ on this graph.

we can rely on the attenuation values, all samplers appear to be linear over the measured range except at the lowest input power.

During the sampler linearity measurements the uncorrelated receiver noise calibration signals were switched at a 1 Hz rate, and separate spectra were recorded with the cal on and off. From these two spectra and the laboratory value of the calibration signals for each receiver channel we can compute the system temperature for each of the 512 channels in each spectrum. The median system temperature for each IF channel as a function of spectral output power is shown in Figure 5. The horizontal axis in Figure 5 is the same as the vertical axis in Figure 4.

As one would expect from the non-linearity at the lowest power points in Figure 4, the measured system temperature is significantly higher for the lowest sampler input power. A weak dependence of system temperature on sampler input power is seen at higher powers which indicate a change in the slope of the transfer function of about 0.2% per dB of input power change. This did not affect our polarization measurements significantly.

7. SUBTLE SYSTEM PROBLEMS AND/OR SURPRISES

7.1. INTERACTION BETWEEN THE CCAL AND UCAL

At 1.4 GHz, our 140-foot system had both an uncorrelated and a correlated cal, i.e. a UCAL and a CAL. The idea was to use the UCAL for amplitude calibration and the CCAL for phase

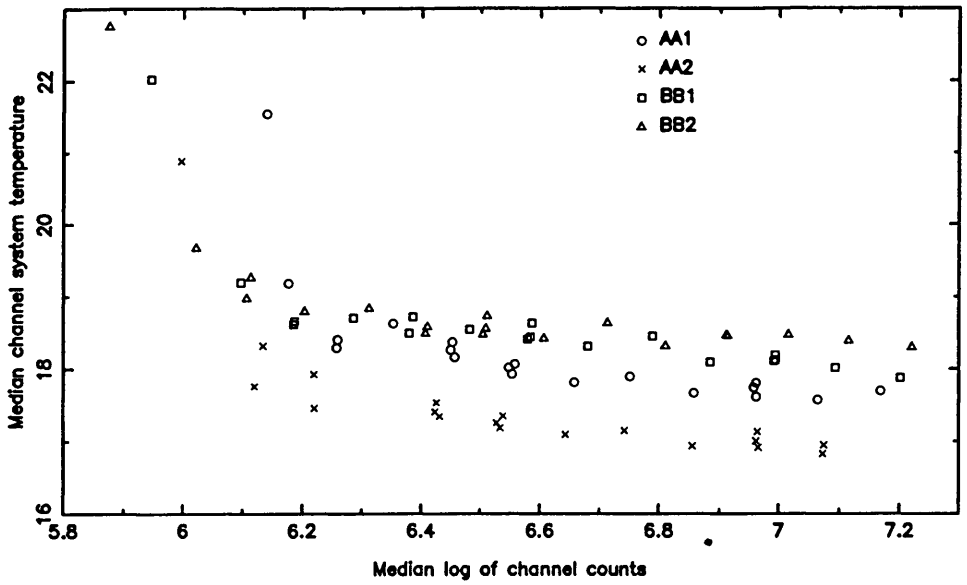

Fig. 5.— Measure system temperature as a function of spectrum output power. The normal operating point for the A/D's is at $log(outputpower) \approx 6.55$ on this graph.

calibration. However, these cals interacted. Both the apparent amplitude and phase of the CCAL were affected by the UCAL being turned on (Here, "phase of the CCAL" means the relative phase between the two polarization channels **X** and **Y**.). Figure 6 shows this dependence in one of the IF's. Here, the solid line at the top is the CCAL deflection with the UCAL off and the dashed line just below is the CCAL deflection with the UCAL on; this difference is about 3.3%. At the bottom, the solid line is the UCAL deflection with the CCAL off and the dashed line is the UCAL deflection with the CCAL on; this difference is about 15%. The ratio of these percentage differences is roughly equal to the ratio of the "other" cal intensities. This suggests a saturation effect; however, the middle sawtooth shows the system temperature changing on and off three astronomical sources. The sources have zero effect on the cal deflections, and the largest source raises the system temperature by 14 K—about 2.5 times larger than the CCAL. Thus it is not a saturation effect.

Not only does the UCAL affect the amplitude of the CCAL, but Figure 7 shows that it also affects the phase. The phase of the CCAL changes by 0.9 degrees when the UCAL is turned on. The phase is unaffected by a simple increase in system temperature from an astronomical source.

It is not easy to understand the reason for this interdependence. However, it exists. Given this inescapable fact for this particular system, we cannot be confident of an absence of interdependence in *any* future system.

This need not be a problem. As we discussed in sections 3.2 and 4.9, there is no reason to use two different cals. At Arecibo we used only a CCAL. The phase of the CCAL was adjusted

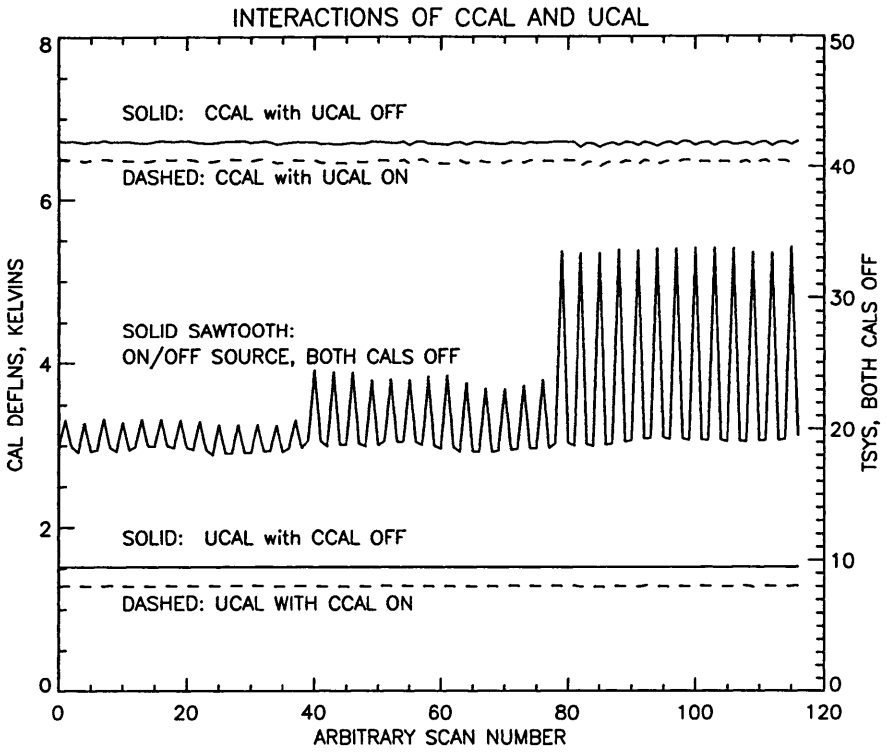

Fig. 6.— CCAL and UCAL deflections with the other cal both on and off for IF0, versus scan number (with arbitrary zero subtracted). The left-hand vertical axis is for the upper and lower pairs of solid and dashed lines, which show the CCAL and UCAL deflections with both the other cal both on and off. The right-hand vertical axis is the total system temperature: While these measurements were going on, the telescope was moving on and off continuum sources and the total system temperature was changing, shown by the solid sawtooth.

to provide approximate linear polarization, with $\Delta\phi = \phi_{SRC} - \phi_{CCAL} \approx 2°$. This turned out to be a very convenient situation because it made the Mueller matrix elements m_{VU}, m_{UV} small and thereby simplified the calibration. We note, however, that making $\Delta\phi$ small is not essential.

One more point. The interaction between GB's CCAL and UCAL underscores the desirability of following the basic philosophical tenet in astronomical measurements, to wit: never measure more than one signal at a time. Thus, when calibrating, use only one calibrator at a time. And more importantly, when observing, never inject the extraneous calibration signal. Injecting excess noise for calibration purposes not only increases the system temperature, but it also puts the system slightly off balance, moving it away from the operating point at which it was calibrated. In

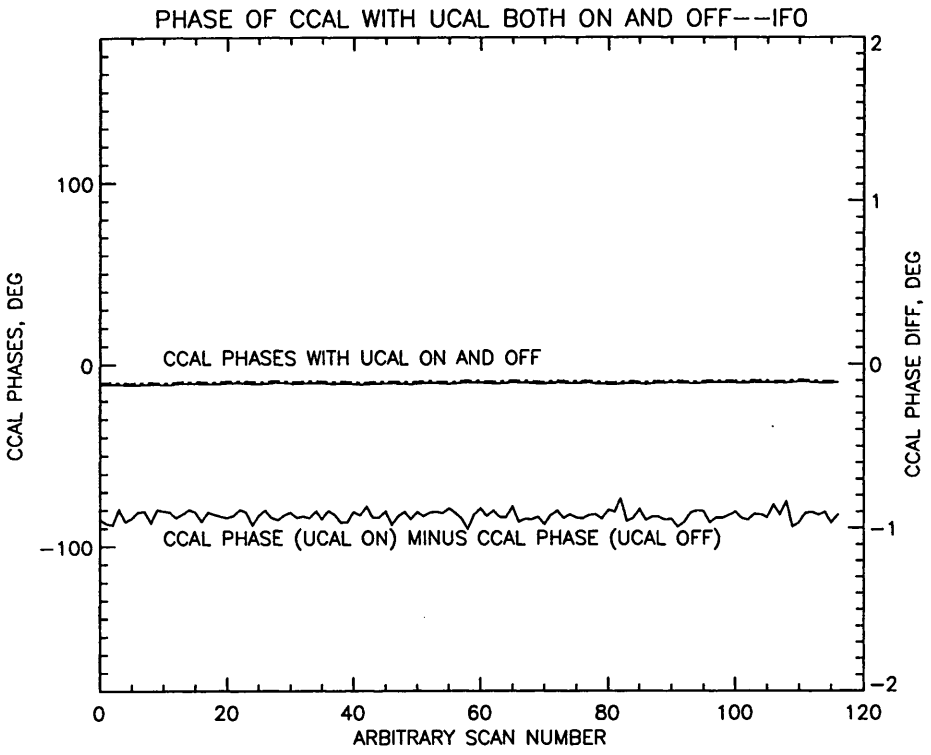

Fig. 7.— CCAL phase with the UCAL both on and off for IF0. The left-hand vertical axis is for the solid and dashed lines, almost superposed, which show the CCAL phases with the UCAL both on and off. The right-hand axis is for the phase difference between these states, shown by the wiggly solid line. The arbitrary scan numbers are the same as those in Figure 6, and the constancy of the CCAL phase difference indicates that it is unaffected by system temperature variations.

other words, one should compare the source deflection S with the cal deflection C. This departs from the past NRAO practice, used in the 140-foot 1024-channel autocorrelator, of comparing $S + C$ with C.

7.2. NONZERO XY FOR AN UNPOLARIZED SOURCE

As discussed in section 8.1, the A_U coefficient of the least square fit for the position angle variation of the Stokes U in equation 36b represents the Mueller matrix element m_{UI}. One uses a similar equation to find m_{VI}.

These imperfections impact spectral polarimetry measurements, as most easily illustrated

with the absorption spectrum of a strong unpolarized source. Figure 8 shows the example of the 21-cm line absorption spectrum against Cas A. Cas A is polarized to only a very small degree—we measured it to be $\sim 0.19\% \pm 0.06\%$ polarized during our continuum source survey. However, in the spectral measurement there are much larger $\sim 1\%$ replicas of the absorption line in the **XY** spectra. In the Re(**XY**) spectrum the source goes positive (m_{UI}), making the absorption line look negative, and the Im(**XY**) spectrum is the other way around (m_{VI}).

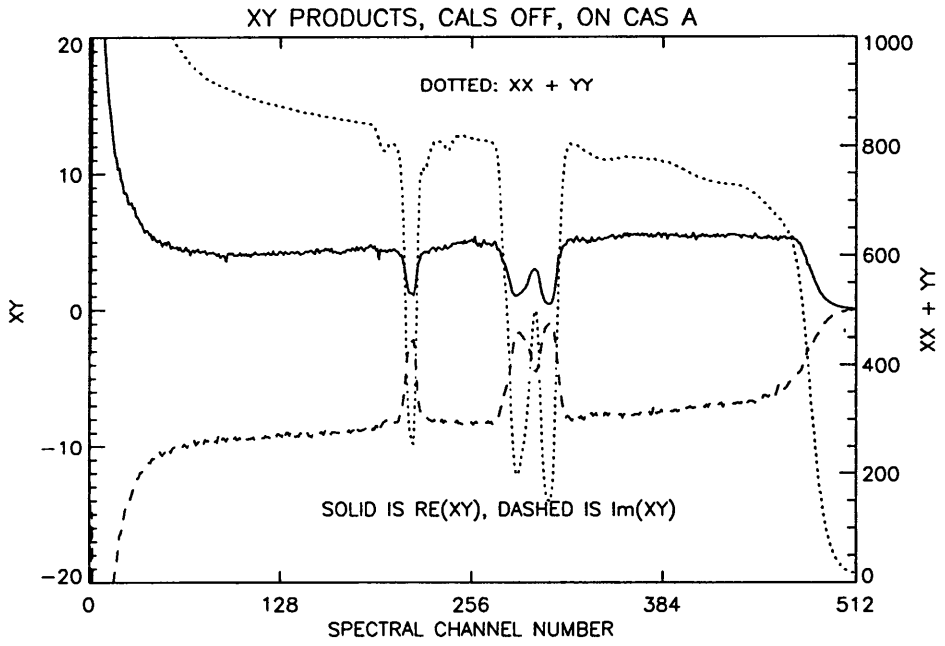

Fig. 8.— 21-cm line absorption against Cas A, 1.25 MHz bandwidth. The left-hand vertical scale is for the **XY** products and the right-hand scale for **XX** + **YY**.

When observing Zeeman splitting, classically one removes the effect for the line *alone* in a least-square fitting process. There are two advantages of knowing and correcting for the Mueller matrix. Firstly, this after-the-fact empirical correction becomes much smaller. Secondly, correcting for the matrix elements removes artifacts from not only the line but also the continuum. For example, Figure 8, shows that there are nonzero **XY** products lying outside the line whose spectral shape mimics the shape of the spectral processor's input filters. These are mostly removed with the Mueller matrix correction.

7.3. NONZERO XY WHEN NO SOURCE IS BEING OBSERVED

Nonzero **XY** products also occur when observing no source whatsoever, at the $\sim 1\%$ level. Figure 9 shows the normalized **XY** spectra of these nonzero products with 10 MHz bandwidth. Here the amplitudes of the two **XY** products follow the bandpass shape quite closely, particularly at the ends, and also the phase varies much more rapidly with frequency than does the CCAL deflection. Again, these rapid frequency variations strongly imply that this residual correlation occurs within the spectral processor itself.

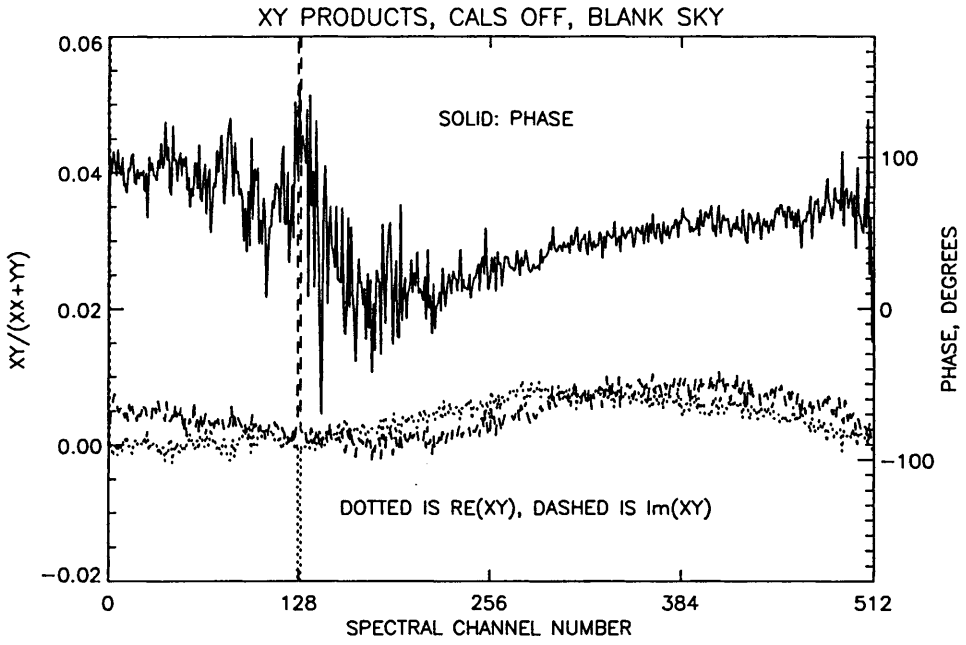

Fig. 9.— XY spectra of system noise, with no correlated input noise, for 10 MHz bandwidth. The two **XY** products are normalized to the sum **XX** + **YY** and are shown by dotted and dashed lines. The left-hand vertical axis gives the scale for the intensity of the two products and the right hand their relative phase, which is shown by the solid line. The spike at channel 128 is the correlated signal from the vertex radiator.

This effect has no obvious ramifications for observing except that the astronomer should do on-off measurements to subtract it away—and one *needs to* subtract it away. It is important to be aware of this because otherwise one might be tempted to rely on the cross-correlation being good enough to eliminate the necessity for an "off".

7.4. LOSS OF CORRELATION FOR CORRELATED SIGNALS IN THE SPECTRAL PROCESSOR

The spectral processor is known to lose some correlation on correlated signals. This means that the **XY** outputs are smaller than they should be. In Mueller matrix terms, this means that $(m_{UU}, m_{VV}) < 1$.

We noticed this effect on our survey of linear polarization of astronomical sources. We derived the linearly polarized flux by least squares fitting observations at twelve different position angles (covering a range of 360°, spaced by 30°). We used two different data sets: one was the difference between the source deflections in the orthogonally polarized feeds and the other was the deflection of the correlated signal of the two feeds. Both sets should measure the same thing, except that the position angles on the sky differ by 45°. However, the polarized fluxes from the correlated signal were systematically smaller than from the difference. This is evident in Table 1, which lists our results: for sources with two listings observed during Jan99, the first line shows results derived from the difference and the second from the cross product.

For a straight average of the 18 sources having significant polarized flux, the cross product polarized fluxes were systematically smaller than the difference fluxes by 8.3% ± 1.5%. In other words, $(m_{UU}, m_{VV}) \sim 0.92$. From the practical standpoint of astronomical measurements, this is an unfortunate but not terribly serious effect. All polarized fluxes should be increased by this amount and the signal/noise is degraded somewhat.

8. A SURVEY OF LINEAR POLARIZED SOURCES AT 1420 MHZ

8.1. THE LEAST SQUARES FIT TO POSITION ANGLE

Suppose a linearly polarized source has polarized intensity P_s and position angle θ_s. Then the two linear-polarized Stokes parameters are

$$Q_s = P_s \cos(2\theta_s) \tag{34a}$$

$$U_s = P_s \sin(2\theta_s)\,. \tag{34b}$$

If we observe this source with our orthogonally linearly polarized feeds oriented at angle PA, then it is clear that the observed Q and U are

$$Q_{obs} = Q_s \cos(2PA) + U_s \sin(2PA) \tag{35a}$$

$$U_{obs} = -Q_s \sin(2PA) + U_s \cos(2PA) \,. \tag{35b}$$

Here, Q_{obs} is obtained from the difference between intensity $(\mathbf{XX} - \mathbf{YY})$ and U_{obs} from $\mathbf{XY}$.

If we do least squares fits as follows:

$$Q_{obs} = A_Q + B_Q \cos(2PA) + C_Q \sin(2PA) \tag{36a}$$

$$U_{obs} = A_U + B_U \cos(2PA) + C_U \sin(2PA) \,, \tag{36b}$$

then by simple identification on a term-by-term basis we have

$$Q_s = B_Q = -C_U \tag{37a}$$

$$U_s = C_Q = B_U \,. \tag{37b}$$

In the ideal world, $A_Q = A_U = 0$. In the real world, they are nonzero. For a dual-linear feed, the departure of A_Q from zero (a nonzero m_{QI}) is a simple scale error in the relative calibration of $\mathbf{XX}$ and $\mathbf{YY}$. The departure of A_U from zero (a nonzero m_{UI}) indicates a residual $\mathbf{XY}$ correlation.

8.2. DERIVING P_s AND θ_s: PROPAGATION OF ERRORS

This is basic statistical analysis; for an arbitrary result $R_{(B,C)}$ the fundamental equation is $\sigma(R)^2 = [\frac{\delta R}{\delta B}^2 \sigma(B)^2 + \frac{\delta R}{\delta C}^2 \sigma(C)^2]$. So firstly, for the source's polarized intensity $P_s = (B^2 + C^2)^{1/2}$, we have

$$\sigma(P_s)^2 = \frac{B^2\sigma(B)^2 + C^2\sigma(C)^2}{(B^2 + C^2)} \tag{38}$$

and for the particular special case in which $\sigma(B) = \sigma(C)$, then we have

$$\sigma(P_s)^2 = \sigma(B)^2 \,. \tag{39}$$

Secondly, for the position angle given by $\tan(2\theta_s) = \frac{B}{C}$, we have

$$\sigma(2\theta_s)^2 = \frac{B^2\sigma(C)^2 + C^2\sigma(B)^2}{(B^2+C^2)^2} \tag{40}$$

and, for the same special case with $\sigma(B) = \sigma(C)$, we have

$$\sigma(2\theta_s)^2 = \frac{\sigma(B)^2}{(B^2+C^2)} \cdot \tag{41}$$

This research has made use of data from the University of Michigan Radio Astronomy Observatory which is supported by funds from the University of Michigan. Carl Heiles is supported by an NSF grant.

REFERENCES

Aller, H.D., Aller, M.F., Hughes, P.A. 1996, in Blazar Continuum Variability, Astronomical Society of the Pacific Conference Series, 1996, 110, 208.

Bridle, A.H., Davis, M.M., Fomalont, E.G., and Lequeux, J. 1972, AJ, 77, 405.

Conway, R.G. and Kronberg, P.P. 1969, MNRAS, 142, 11

Heiles, C. 1999, Arecibo Observatory Technical Memos 99-01 and 99-02 (web access: Arecibo's website under *Technical Memos, Telescope Performance*, now at *http://naic.edu/ donna/performance.html*).

Kuhr, H., Witzel, A., Pauliny-Toth, I.I.K., Nauber, U. 1981, A&A Suppl, 45, 367.

Stennis, M. 1999, Technical data sheet for 8-10 GHz receiver on 140-foot telescope.

Stinebring, D. 1982, thesis, Cornell University.

Tinbergen, J. 1996, Astronomical Polarimetry, Cambridge University Press.

Table 1. POLARIZATION RESULTS: SOME SINGLE-DISH CALIBRATORS AT 1420 MHZ

Source	α_{1950}	δ_{1950}	S, Jy	P_s, Jy	%Pol	θ_s
3C27	00 52 44.9	68 06 06	6.65	0.93	7.02 ± 0.03	131.9 ± 0.5
3C27	00 52 44.9	68 06 06	6.65	0.82	6.15 ± 0.35	131.8 ± 1.8
3C27 sp	00 52 44.9	68 06 06	6.65	0.52	3.9± ···	122.3± ···
3C29	00 55 00.7	–01 40 30	5.21	1.15	11.01 ± 0.65	171.6 ± 0.4
3C29	00 55 00.7	–01 40 30	5.21	1.10	10.52 ± 0.28	171.6 ± 0.4
3C33	01 06 14.2	13 03 37	12.53	1.81	$7.09 \pm 0.42^*$	$68.6 \pm 0.9^*$
3C33	01 06 14.2	13 03 37	12.53	1.76	$6.92 \pm 0.35^*$	$67.4 \pm 0.7^*$
3C41 AO	01 23 54.7	32 57 36	3.5	0.42	6.0	48.9
3C98	03 56 11.0	10 17 41	10.25	1.05	5.10 ± 0.15	72.0 ± 0.8
3C98	03 56 11.0	10 17 41	10.25	0.96	4.70 ± 0.10	71.0 ± 0.6
3C123	04 33 55.2	29 34 14	45.16	0.45	$0.50 \pm 0.19^*$	$140.2 \pm 5.5^*$
3C123	04 33 55.2	29 34 14	45.16	0.33	$0.36 \pm 0.13^*$	$153.4 \pm 5.1^*$
3C138	05 18 16.5	16 35 26	8.88	1.11	6.81 ± 0.41	176.2 ± 1.1
3C138	05 18 16.5	16 35 26	8.88	1.05	6.48 ± 0.11	176.9 ± 0.3
3C144-TAU	05 31 31.0	21 59 17	895.50	14.68	0.82 ± 0.08	87.9 ± 1.6
3C144-TAU	05 31 31.0	21 59 17	895.50	13.92	0.75 ± 0.09	86.0 ± 2.5
ORION-A	05 32 44.0	–05 24 54	389.65	0.86	0.11 ± 0.10	···
ORION-A	05 32 44.0	–05 24 54	389.65	0.94	0.12 ± 0.14	···
3C147.1	05 39 11.0	–01 55 36	57.78	0.69	$0.60 \pm 0.30^*$	$84.0 \pm 7.2^*$
3C147.1	05 39 11.0	–01 55 36	57.78	0.68	$0.59 \pm 0.10^*$	$84.5 \pm 2.4^*$
P0736+01 AO	07 36 42.6	01 44 00	2.9	0.48	8.2	103.4
3C227	09 45 07.8	07 39 09	7.18	0.74	5.14 ± 0.37	142.4 ± 1.0
3C227	09 45 07.8	07 39 09	7.18	0.66	4.56 ± 0.06	144.8 ± 0.7
3C227 sp	09 45 07.8	07 39 09	7.18	0.47	3.3± ···	146.7± ···

Table 1—Continued

Source	α_{1950}	δ_{1950}	S, Jy	P_s, Jy	%Pol	θ_s
3C270	12 16 51.2	06 06 13	17.20	2.62	7.62 ± 0.30	122.1 ± 2.3
3C270	12 16 51.2	06 06 13	17.20	2.63	7.63 ± 0.17	122.3 ± 1.5
3C270 sp	12 16 51.2	06 06 13	17.20	2.22	6.3± ···	128.1± ···
3C273	12 26 32.9	02 19 39	49.77	1.23	1.24 ± 0.04	149.7 ± 0.9
3C273	12 26 32.9	02 19 39	49.77	1.17	1.17 ± 0.06	151.0 ± 0.7
3C274	12 28 17.8	12 39 50	213.56	4.27	1.00 ± 0.05	144.5 ± 5.6
3C274	12 28 17.8	12 39 50	213.56	3.89	0.91 ± 0.09	144.5 ± 6.3
3C274.1	12 32 57.0	21 37 06	2.64	0.77	14.52 ± 1.70*	149.9 ± 1.7*
3C274.1	12 32 57.0	21 37 06	2.64	0.61	11.61 ± 0.37*	152.6 ± 0.5*
3C274.1 AO	12 32 57.0	21 37 06	2.64	0.67	12.8	158.6
3C286	13 28 49.7	30 46 02	14.78	2.74	9.52 ± 0.16	27.4 ± 0.1
3C286	13 28 49.7	30 46 02	14.78	2.60	9.04 ± 0.13	27.4 ± 0.2
3C286 AO	13 28 49.7	30 46 02	14.78	2.86	9.7	28.8
3C286 sp	13 28 49.7	30 46 02	14.78	2.34	7.9± ···	34.3± ···
P1414+11	14 14 27.3	11 02 16	4.14	0.82	9.89 ± 0.22	25.4 ± 3.1
P1414+11	14 14 27.3	11 02 16	4.14	0.78	9.45 ± 0.15	26.4 ± 0.2
3C336 AO	16 22 33.5	23 52 06	2.7	0.15	2.7	29.1
3C348	16 48 40.1	05 04 28	43.69	1.37	1.57 ± 0.17*	57.0 ± 1.5*
3C348	16 48 40.1	05 04 28	43.69	1.27	1.45 ± 0.09*	57.1 ± 0.8*
3C348 sp	16 48 40.1	05 04 28	43.69	1.31	1.5± ···	68.1± ···
M17	18 17 33.0	40 35 02	558.25	9.60	0.86 ± 0.02	81.4 ± 1.3
M17	18 17 33.0	40 35 02	558.25	8.49	0.76 ± 0.02	82.8 ± 0.7
W43	18 44 57.0	–01 56 36	140.50	3.04	1.08 ± 0.15*	85.1 ± 1.9*
W43	18 44 57.0	–01 56 36	140.50	2.78	0.99 ± 0.12*	86.5 ± 1.7*
3C399.1 AO	19 14 00.0	30 14 23	2.7	0.56	10.3	53.6
3C405-CYG	19 57 44.5	40 35 02	1654.90	16.88	0.51 ± 0.05	175.7 ± 6.3
3C405-CYG	19 57 44.5	40 35 02	1654.90	17.54	0.53 ± 0.06	178.3 ± 1.5

Table 1—Continued

Source	α_{1950}	δ_{1950}	S, Jy	P_s, Jy	%Pol	θ_s
3C433 sp	21 21 30.6	24 51 18	11.68	1.67	7.1± ···	136.0± ···
CTA102 sp	22 30 07.7	11 28 23	6.37	0.65	5.1± ···	105.3± ···
3C452 sun	22 43 33.0	39 25 28	14.40	2.74	9.52 ± 0.16	27.4 ± 0.1
3C452 sun	22 43 33.0	39 25 28	14.40	2.60	9.04 ± 0.13	27.4 ± 0.2
3C452 sp	22 43 33.0	39 25 28	9.71	1.22	6.3± ···	13.9± ···
3C454.3	22 51 29.4	15 52 56	13.56	2.09	$7.69 \pm 0.55^*$	$67.8 \pm 1.0^*$
3C454.3	22 51 29.4	15 52 56	13.56	1.81	$6.67 \pm 0.22^*$	$68.0 \pm 0.5^*$
3C454.3 AO	22 51 29.4	15 52 56	13.56	1.57	5.8	70.6
CAS-A	23 21 07.0	58 33 48	2032.00	10.97	0.27 ± 0.18	4.2 ± 8.8
CAS-A	23 21 07.0	58 33 48	2032.00	7.72	0.19 ± 0.06	4.5 ± 2.7

Note. — Column 1 is the source name, column 2 and 3 the 1950 equatorial coordinates, column 4 the flux density S in Jy ($S = \frac{\text{Stokes } I}{2}$), column 5 the polarized flux density $P_s = (Q_s^2 + U_s^2)^{1/2}$ in Jy, column 6 the percent polarization (defined as $\frac{100 P_s}{2S}$), column 7 the position angle.

Note. — Sources listed twice were observed during Jan 99. The first listing was derived from the Stokes Q (the difference between orthogonal linear polarizations) and the second from the Stokes U (the cross-correlation of the two linears). The letters "sp" means that the source was observed during the Spring 1998 observing period; uncertainties are not available and the data somewhat less accurate than in Jan 1999. "sun" means that the observations were severely affected by the Sun and should not be trusted, and in particular that the errors are almost certainly underestimates.

Note. — Most results were derived from at least two 12 position angle datasets at the 140-foot telescope. For them, the quoted errors are derived from the differences among those datasets. For results whose errors have the superscript * there was only a single 12 position angle dataset and the quoted errors are too small.

Note. — Sources followed by "AO" were observed at Arecibo during Feb99; their results should be more accurate than the 140-foot results.

Table 2. SOME SINGLE-DISH CALIBRATORS AT 4.8, 8.0, and 14.5 GHZ

Source	α_{1950}	δ_{1950}	$S_{4.8}$	$S_{8.0}$	$S_{14.5}$	$P_{4.8}$	$P_{8.0}$	$P_{14.5}$	$\theta_{4.8}$	$\theta_{8.0}$	$\theta_{14.5}$
NRAO5	00 03 40.3	-06 40 17	2.2	2.7	2.3	3.5	3.5	5.0	40	20	20
3C48	01 34 49.8	32 54 21	5.40	3.56	1.84	4.02	5.17	6.62	104.0	113.7	115.2
3C58	02 01 52.0	64 35 06	29.3	28.0	23.1	5.6	5.5	5.5	163	177	7
3C66B	02 20 01.9	42 45 54	3.26	1.78	0.81	3.63	3.6	2.5	70.5	79.	94.
P0218+35.7	02 18 04.1	35 42 32	1.3	1.2	1.2	2.5	2.0	7.0	20	40	50
3C10	02 22 32.0	63 51 42	15.5	8.0	1.7	0.5	1.0	2.5	110	140	110?
3C83.1	03 15 00.0	41 41 12	1.8	1.1	0.6	5.5	6.0	6.5	110	115	120
3C84	03 16 29.6	41 19 52	22	21	19	0.05	0.05	0.05	—	—	—
NRAO140	03 33 22.6	32 08 37	1.6	1.4	1.7	4.0	4.5	3.0	60	45	50
3C93	03 40 51.6	04 48 22	0.87	0.59	0.32	7.5	7.4	10.6	139.2	131.	134.
4C76.03	04 03 58.6	76 48 54	2.8	2.2	1.5	0.5	2?	3.0	0	100?	50
3C138	05 18 16.5	16 35 27	3.8	2.8	1.5	10.5	11.0	11.0	170	170	170
P0521-36.5	05 21 12.9	-36 30 17	8.0	7.5	5.0	3.5	2.2	2.0	75	70	70
3C144	05 31 31.0	21 59 17	596	560	430	5.0	6.8	9.9	141	146	152
3C147	05 38 43.5	49 49 43	7.5	5.5	2.8	0.3	1.0	3.0	0	150	50
3C153	06 05 44.5	48 04 49	1.32	0.81	0.40	3.94	5.1	5.2	52.3	50.	54.
3C196	08 09 59.4	48 22 07	4.3	2.6	1.2	2.3	2.0	2.0	120	150	160
P0836+71.0	08 36 21.5	71 04 22	2.3	2.6	2.3	7.0	4.8	4.0	100	105	125
3C207	08 38 01.8	13 23 06	1.3	1.3	1.3	3.0	3.0	2.0	25	20	15
3C216	09 06 17.3	43 05 59	1.6	1.3	1.1	1.5	1.5	2.0	90	0	150
3C219	09 17 50.7	45 51 44	2.4	1.4	0.8	3.0	4.0	2.5	145	140	130
3C245	10 40 06.1	12 19 15	1.61	1.33	0.98	8.38	7.00	5.10	33.0	27.9	29.4
P1127-14.5	11 27 35.7	-14 32 55	3.8	3.3	2.6	3.5	3.5	3.0	160	160	160
3C273	12 26 33.2	02 19 43	37	44	48	3.3	3.5	3.0	170	155	148
3C274	12 28 17.6	12 40 02	71	49	29	0.48	1.6	2.9	40	87	53
3C280	12 54 41.4	47 36 32	1.66	1.07	0.54	7.64	8.2	11.2	44.2	51.2	53.2
3C286	13 28 49.7	30 45 59	7.37	5.53	3.53	11.09	11.46	11.82	33.21	33.13	35.21
3C330	16 09 16.2	66 04 30	2.24	1.32	0.64	3.59	4.2	4.0	131.5	132.	108.
MK-501	16 52 11.8	39 50 25	1.6	1.6	1.3	2.7	3.0	3.0	10	5	0
3C353	17 17 55.6	-00 55 54	22.2	15.5	—	5.2	4.4	—	87	79	—
3C390.3	18 45 45.5	79 42 45	4.4	3.1	1.5	6.0	7.0	4.0	25	25	25
3C395	19 01 02.2	31 55 12	1.5	1.5	1.3	4.0	3.5	3.5	65	45	30
P2005+40.3	20 04 13.1	40 20 34	2.7	2.2	1.8	4.5	2.5	2.5	20	50	60
P2014+37.0	20 14 34.6	37 05 03	3.5	2.5	0.9	7.0	7.0	7.0	103	125	135
3C452	22 43 32.8	39 25 28	3.14	1.82	0.63	7.14	7.0	5.9	121.4	159.6	173.

Note. — Column 1 is the source name, column 2 and 3 the 1950 equatorial coordinates, column 4-6 the flux density in Jy ($S = \frac{\text{Stokes } I}{2}$), columns 7-9 the percentage polarization (defined as $\frac{100 \times \text{polarized intensity}}{2S}$), columns 10-12 the position angle in degrees. Subscripts indicate frequency in GHz.

Note. — We perused the University of Michigan catalog (Aller et al 1996) and include all reasonably strong sources whose polarization properties have not varied terribly much over the period 1990 → 1999.0. Sources with names in boldface are stable and have typical uncertainties equal to a few or less in the last quoted decimal place; these values were kindly provided by Hugh Aller. For the others, values were estimated by eye from graphs and uncertainties are at least a few 0.1% in S, a few 0.1% in P, a few degrees in θ; some sources exhibit distinct time variability and the user should check with recent observations. Most positions are from Kuhr et al (1981); some are from BDFL and Simbad. The Michigan database is on the web: *http://www.astro.lsa.umich.edu:80/obs/radiotel/radiotel.html*.